Mechanical Heterogeneity in Tissues Promotes Rigidity and Controls Cellular Invasion

Xinzhi Li,* Amit Das, and Dapeng Bi
Department of Physics, Northeastern University, Boston, Massachusetts 02115, USA

(Received 18 March 2019; revised manuscript received 5 June 2019; published 31 July 2019)

We study the influence of cell-level mechanical heterogeneity in epithelial tissues using a vertex-based model. Heterogeneity is introduced into the cell shape index (p_0) that tunes the stiffness at a single-cell level. The addition of heterogeneity can always enhance the mechanical rigidity of the epithelial layer by increasing its shear modulus, hence making it more rigid. There is an excellent scaling collapse of our data as a function of a single scaling variable f_r, which accounts for the overall fraction of rigid cells. We identify a universal threshold f_r^* that demarcates fluid versus solid tissues. Furthermore, this rigidity onset is far below the contact percolation threshold of rigid cells. These results give rise to a separation of rigidity and contact percolation processes that leads to distinct types of solid states. We also investigate the influence of heterogeneity on tumor invasion dynamics. There is an overall impedance of invasion as the tissue becomes more rigid. Invasion can also occur in an intermediate heterogeneous solid state that is characterized by significant spatial-temporal intermittency.

DOI: 10.1103/PhysRevLett.123.058101

Heterogeneity amongst cells in a tumor has been recognized as one of the hallmarks of cancer [1–4]. This so-called intratumor heterogeneity is thought to facilitate metastasis [1,5,6] by allowing a cellular community the flexibility and efficiency to adapt to new environments [7]. It is also largely responsible for therapeutic resistance [1,2,8,9]. Cellular differences within a tumor result from an interplay of both genetic and extrinsic influences [10–14]. Whereas fitness or genotypic heterogeneity has been studied extensively, the role of mechanical heterogeneity in a tumor or cellular collective is still not well understood.

Recent experimental evidence [15–18] has revealed that tumor cells exhibit a broad distribution of various biomechanical properties. These include intratumor heterogeneity in cell stiffnesses [17,19–22], stresses [23], and cell-cell interactions [21,24]. However, there is no consensus on how these heterogeneities affect the mechanical behavior at the tissue level. For example, while biophysical techniques [25] such as AFM [22] and the optical stretcher [18] show that individual cancer cells are softer than healthy cells, there is an apparent paradox with measurements at the tissue level that tumors are more rigid than healthy tissues [26,27].

From a theoretical or modeling perspective, there is a lack of understanding of how cell-level heterogeneity influences the mechanical state of the tissue. One large class of vertex-based models [28–30] has been used to study mechanics of *homogeneous* epithelial tissues which can exhibit a solid-to-fluid transition [31–39]. However, previous works often treat heterogeneity as biological noise, and therefore they are not well suited to model many of the salient features in tumors.

In this Letter, we study explicitly the effect of heterogeneity on the mechanics of the confluent cell monolayer using the vertex model. Our results show that heterogeneity always enhances the rigidity of a tissue. The mode of enhancement depends on the spatial distribution of rigid vs soft cells, which is directly tuned by a single universal parameter f_r. This results in distinct mechanical regimes that arise from the mismatch of two percolation processes: (1) rigidity percolation of mechanical tensions and (2) contact percolation of rigid cells. We also connect tissue rigidity to cellular migration using a model for the invasion of a single metastatic cell in a heterotypic microenvironment of the tissue. The burstlike intermittency in the heterogeneous solid state is highly reminiscent of the pulsating cancer cell migration recently observed in epithelial monolayers [24].

Model.—In the vertex model, a 2D confluent epithelial tissue is governed by the energy function [28–31,33,40] $E=\sum_{i=1}^{N}[K_A(A_i-A_0^i)^2+K_P(P_i-P_0^i)^2]$, where cell areas $\{A_i\}$ and perimeters $\{P_i\}$ are functionals of the positions of vertices $\{\mathbf{r}_i\}$. K_A and K_P are the area and perimeter elasticities. The term quadratic in A_i results from resistance to cell volume changes [29–31]. Changes to cell perimeters are related to the deformation of the actomyosin cortex [41,42]. The term $K_P P_i^2$ corresponds to the energy cost of deforming the cortex. The linear term, $-2K_P P_0^i P_i$, is the effective line tension by cell i which gives rise to a "preferred perimeter" P_0^i. The value of P_0^i emerges from an interplay of cell-cell adhesion and cortical tension [29,31,32,43]. Here we assume the preferred cell area A_0 does not vary from cell to cell and is set to be the average area per cell ($A_0^i = \bar{A}$). The energy can be nondimensionalized by choosing $K_P\bar{A}$ as the energy unit and $\sqrt{\bar{A}}$ as the length unit

$$\varepsilon = \sum_{i=1}^{N} [\kappa_A (a_i - 1)^2 + (p_i - p_0^i)^2], \tag{1}$$

where $a_i = A_i/\bar{A}$ and $p_i = P_i/\sqrt{\bar{A}}$ are the rescaled area and perimeter of the ith cell. $\kappa_A = K_A\bar{A}/K_P$ is the rescaled cell area elasticity, and $p_0^i = P_0^i/\sqrt{\bar{A}}$ is the preferred *cell shape index* [32].

In this model, the cell stiffness is determined by the tension τ_m on cell-cell junctions (edges) [44–50]. For an edge with length l_m, the tension is given by [51,52]

$$\tau_m \equiv \frac{\partial \varepsilon}{\partial l_m} = (p_i - p_0^i) + (p_j - p_0^j), \tag{2}$$

where p_i and p_j are the rescaled perimeters of cells i, j adjacent to the edge m. As a result, the cell stiffness is directly tuned by the preferred cell shape indices. To capture the experimental heterogeneities in single-cell stiffnesses and in cell-cell interactions [17,19–22], we introduce variations in the preferred shape indices $\{p_0^i\}$. The majority of this work uses a Gaussian distributed set of $\{p_0^i\}$ with mean μ and standard deviation σ. The results are insensitive to the form of distribution for $\{p_0^i\}$ (see the Supplemental Material (SM) [53]).

To initialize the simulation, Voronoi cells [55,56] are used to provide a set of initial vertex positions, $\{\boldsymbol{r}_i\}$. Then each cell is assigned a value of p_0^i drawn from a Gaussian distribution with mean μ and standard deviation σ. The set of $\{p_0^i\}$ remain as *quenched variables*. We use the open-source SURFACE EVOLVER [57] and a combination of the FIRE and conjugate-gradient [58,59] algorithms to minimize Eq. (1) under periodic boundary conditions (see the SM [53] for a sample script and discussions on the impact of different boundary conditions with Refs. [60–65]). The network topology is updated using $T1$ moves [32,66,67]. This algorithm produces stable states where the net residual force on vertices is $< 10^{-10}$. A range of parameters $\mu = 3.6$–3.95, $\sigma = 0$–0.3, κ_A, and system sizes $N = 36$–900 are studied.

Cellular heterogeneity enhances rigidity.—We first focus on the case where area and perimeter elasticities are matched in their strengths ($\kappa_A = 1$). In Fig. 1(a), the shear modulus G (see the SM [53]) is plotted as a function of μ and σ. At $\sigma = 0$, G vanishes at $\mu \approx 3.828$. This recapitulates the rigidity transition in the absence of heterogeneity [29,32,51]. Increasing σ at fixed μ always enhances the rigidity, which can occur in two different ways: (i) for a rigid tissue when $\sigma = 0$, G always increases with σ, and (ii) for a fluid tissue, $G = 0$ when $0 < \sigma \leq \sigma^*$ but becomes rigid when $\sigma \geq \sigma^*$. The threshold σ^* where rigidity emerges depends on μ. To better understand the dependence of G on (μ, σ), we first hypothesize that σ provides an overall scale for the shear modulus and plot a rescaled G/σ as function of μ for various σ [inset of Fig. 1(a)]. This yields an intriguing result, where all curves

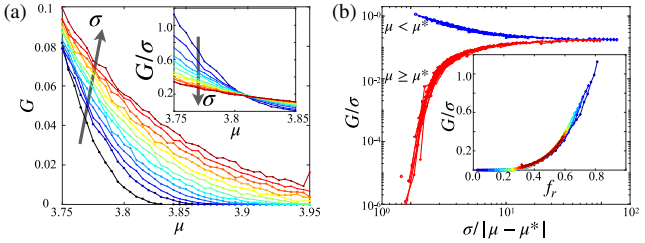

FIG. 1. Tissue mechanical property. (a) Shear modulus G (in units of K_P) vs μ at $\sigma = 0, 0.07, 0.09, 0.11, 0.13, 0.15, 0.17, 0.19, 0.21, 0.23, 0.25, 0.27, 0.29$ for $N = 400$, $\kappa_A = 1$. (Inset) G/σ vs μ. (b) G/σ vs $\sigma/|\mu - \mu^*|$ in log-log scale. (Inset) G/σ vs the fraction of rigid cells f_r [defined in Eq. (4)].

in the inset of Fig. 1(a) intersect at a common point $\mu^* \approx 3.8$. The μ^* serves as a crossover point between two distinct regimes. When $\mu < \mu^*$, G/σ decreases as σ is increased. For $\mu \geq \mu^*$, the behavior is flipped and G/σ *increases* with σ. The intersection of all curves also suggests that closer to μ^*, the shear modulus should converge to a scaling of $G \propto \sigma$. Based on these observations, we hypothesize that the behavior of G below and above μ^* may be described by a universal scaling relation

$$G = \sigma g_{\pm}\left(\frac{\sigma}{|\mu - \mu^*|}\right). \tag{3}$$

We replot all data based on the ansatz [Eq. (3)] in Fig. 1(b). An excellent scaling collapse is obtained, which allows for pinpointing of the location of the crossover transition $\mu^* = 3.812$ separating G/σ into two distinct regimes g_+, g_- where $\pm = \mathrm{sgn}(\mu - \mu^*)$. In Fig. 1(b), all data with $\mu > \mu^*$ (shown in red) collapse onto the g_+ branch. In contrast, data with $\mu < \mu^*$ (shown in blue) correspond to the g_- branch. The two branches meet at $\mu = \mu^*$, where G scales linearly with σ.

The universal scaling near μ^* provides insights into the nature of rigidity. At the crossover μ^*, there are 50% of cells with $p_0^i < \mu^*$ regardless of the value of σ. Below the crossover ($\mu < \mu^*$), cells with $p_0^i < \mu^*$ exceed 50%, while above the crossover ($\mu > \mu^*$) this fraction is below 50%. This suggests that the fraction of cells with $p_0^i < \mu^*$ plays an important role. Therefore we define this fraction as

$$f_r = \int_{-\infty}^{\mu^*} \mathcal{F}_{\mu,\sigma}(p_0) dp_0, \tag{4}$$

where $\mathcal{F}$ is the probability distribution function and for a Gaussian, $f_r = (1/2)\mathrm{erfc}[(\mu - \mu^*)/(\sqrt{2}\sigma)]$. In the inset of Fig. 1(b), a replot of all data in terms of G/σ vs f_r collapses to a common curve. Interestingly, the numerical value $p_0 = 3.812$ was previously found to be the threshold for rigidity in tissues [32] with homogeneous p_0. This universal scaling behavior supports the idea that $p_0^i < \mu^*$ can serve as a *single-cell* criterion for rigidity and their fraction

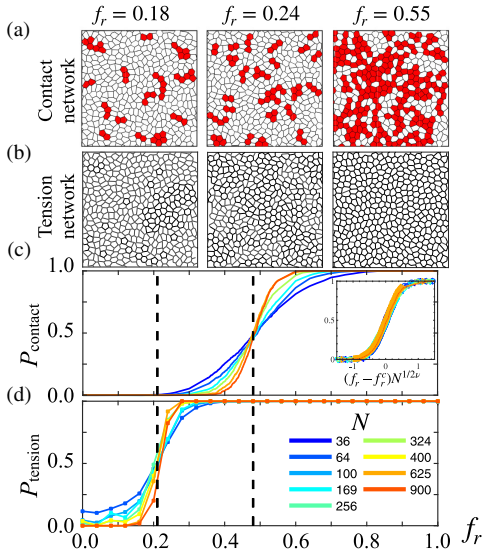

FIG. 2. Rigidity and contact percolations do not coincide. (a) Connected clusters of rigid cells shown in red. White cells correspond to $p_0^i \geq \mu^*$. (b) Typical snapshots for the tension network. Edges with finite tensions are indicated by thick black lines, while other edges have $\tau = 0$. (c) Probability of contact percolation for rigid cells, P_{contact} vs f_r. Colors indicate different tissue sizes in the range $N = 36$–900 (see the SM [53] for the method of calculating P_{contact}). (Inset) Finite-size scaling yields a contact percolation threshold of $f_r^c = 0.475 \pm 0.005$ and $\nu = 1.60 \pm 0.03$. (d) Probability to obtain a system-spanning tension cluster vs f_r. Finite-size analysis yields a transition at $f_r^* = 0.21 \pm 0.01$.

f_r determines tissue mechanics. We therefore refer to f_r as the *fraction of rigid cells*.

Heterogeneity drives two different percolations.—The emergence of rigidity when a certain population of cells exceeds a fraction is reminiscent of a percolation process [68–72]. To test whether f_r drives a percolation transition, we analyze the spatial organization of rigid cells. Snapshots of connected rigid cells are shown in Fig. 2(a), and the probability for rigid cells to form a system-spanning contact network is plotted in Fig. 2(c). Finite-size scaling [inset of Fig. 2(c)] shows a contact percolation transition at $f_r^c = 0.475 \pm 0.005$ with exponent $\nu = 1.60 \pm 0.03$. However, according to the inset of Figs. 1(b) and 3(b), the tissue becomes rigid at a much lower $f_r \approx 0.21$, suggesting the contact percolation of rigid cells is not necessary for rigidity. We then hypothesize that the percolation of the tension network is necessary for rigidity rather than rigid-cell contacts. Figure 2(d) shows tension percolation occurring at $f_r^* = 0.21 \pm 0.01$, coinciding with the rigidity onset. Snapshots of tensions [Fig. 2(b)] highlight an interesting behavior: e.g., at $f_r = 0.24$, the rigid-cell contact network does not span the system, yet tensions form a system-spanning structure. Therefore the presence of just a few unconnected rigid cells can induce a much more spatially extended tension network. The distribution

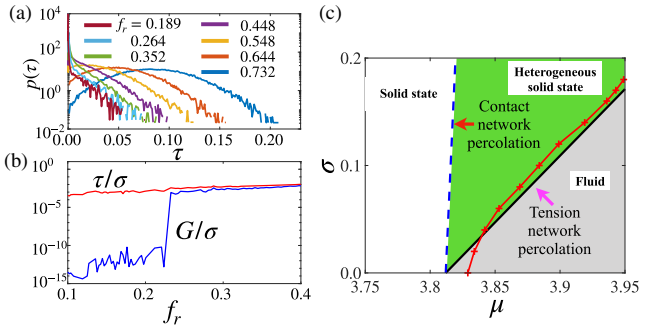

FIG. 3. Spatial distribution of cellular tensions dictates tissue rigidity. (a) Distribution of tensions $p(\tau)$ in semilog scale at $\kappa_A = 1$, $N = 400$ for various f_r. (b) G/σ and τ/σ vs f_r in semilog scale at $\kappa_A = 1$, $\sigma = 0.1$, $N = 400$. G/σ vanishes at $f_r^* = 0.21$, while the tension remains finite even in fluid states. τ has units of $K_P\sqrt{A}$, and G has units of K_P. (c) A phase diagram in (μ, σ). The solid black line indicates rigidity percolation and corresponds to values of μ and σ where $f_r = f_r^*$. The red line is the mean field estimate for the bond percolation on a random Voronoi tessellation. The blue dashed line indicates the contact percolation transition of rigid cells at f_r^c. The mismatch between rigidity and contact percolations results in an intermediate "heterogeneous solid state" which exists only for $\sigma > 0$.

of tensions $p(\tau)$ also evolves as a function of f_r in an unconventional way [Fig. 3(a)]. For values of $f_r > 0.21$ corresponding to rigid states, $p(\tau)$ vanishes as $\tau \to 0$ and appears symmetrical about their mean. At lower f_r, $p(\tau)$ becomes significantly more skewed and heavy tailed (see the SM [53]) and also develops an excess number of $\tau \approx 0$ edges. Interestingly, the average tension for the tissue $\langle\tau\rangle$ does not vanish [Fig. 3(b)] even below f_r^*, and it does not show drastic changes at f_r^*. In contrast, G/σ undergoes a transition at f_r^*, coinciding with the tension network percolation. Remarkably, two states with slight differences in their tensions can differ by several orders of magnitudes in G (see the SM [53] for snapshots), depending on whether the tension network is percolated.

We use a simple mean field approach to estimate the rigidity transition threshold $f_r^* = 0.21$. The network shares a similar topology with random Voronoi tessellations where the *bond percolation* threshold $= 0.66$ [73–75]. Therefore if rigidity requires the percolation of edges with finite tensions, the onset of rigidity should correspond to the time when there are exactly 66% cell edges with finite tensions. For each parameter pair (μ, σ), we define the fraction of finite tensions as $N_\tau = \int_{\tau_0}^{\infty} p(\tau)d\tau$, where the threshold $\tau_0 = 10^{-5}$ is chosen to define "zero" tensions coinciding with the noise floor in the numerical calculations. In Fig. 3(c), we show that the point at which $N_\tau(\mu, \sigma) = 0.66$ is consistent with the rigidity transition, i.e., $f_r^* = 0.21$. Taken together, these results suggest that a *rigidity percolation* occurs at f_r^*.

The mechanics of the tissue is summarized in a phase diagram [Fig. 3(c)]. Solid and fluidlike states are separated by f_r^*, which corresponds to a rigidity percolation of the

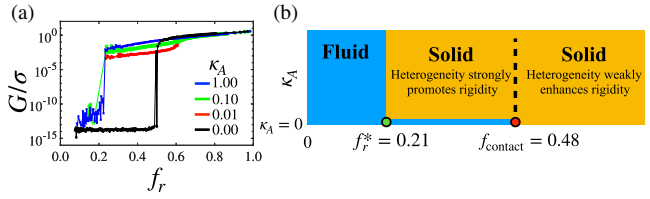

FIG. 4. The effect of heterogeneity depends on cell area elasticity. (a) G/σ vs f_r in semilog scale at various κ_A values. G has unit of K_P. (b) Phase diagram of mechanical property as a function of f_r and κ_A. The rigidity and contact percolations are distinct when $\kappa_A > 0$ but coincide at $\kappa_A = 0$. The region of ($\kappa_A > 0$, $f_r^* < f_r < f_r^c$) corresponds to a solid that follows the lower branch in Fig. 1(b), where the shear modulus is sharply enhanced by increasing heterogeneity.

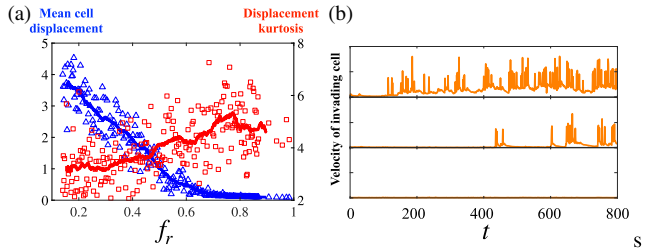

FIG. 5. Heterogeneity and cellular invasion. (a) Analysis of the time-averaged displacement (in units of $\sqrt{A}$) of a single cell attempting to move through the tissue with constant $v_0 = 0.4$ at various f_r. Blue points represent the mean displacement of the cell taken over twice the persistence time. Red points represent the kurtosis of short time displacements indicating a growing intermittency of the invasion dynamics. (b) Representative traces of the invading cell velocities in units of $K_P\sqrt{A}/\Gamma$. (Top panel) The fluid phase at $f_r = 0.14$. (Middle panel) The intermediate solid phase at $f_r = 0.47$. (Bottom panel) The rigid phase when $f_r = 0.98$.

edge tensions. Contact percolation of rigid cells occurs at a higher value of f_r than the rigidity percolation. The mismatch between contact and rigidity percolations can be observed only in the presence of heterogeneity since, at $\sigma = 0$, f_r is either 0 or 1. We call the intermediate region between the two percolation transitions the heterogeneous solid state. Rigidity transition obtained through the mean field method is shown as the red line in Fig. 3(c).

Cell area elasticity κ_A weakens the effect of heterogeneity.—Next we focus on the heterogeneous solid state ($f_r^* < f_r < f_r^c$). The regime is characterized by spatial heterogeneity [Figs. 2(a) and 2(b)], where isolated rigid-cell and tension clusters exist alongside tissue-spanning percolated tension networks. Mechanical force balance must hold at every vertex [51] for a solid tissue. However, for an isolated tension cluster, edge tensions alone cannot guarantee force balance, such as a vertex that sits on the boundary of this cluster. The missing component required for full force balance is the *intracellular pressure* force that acts perpendicularly on an edge given by [51,52] $\Pi_m = \kappa_A(a_i - a_j)$. Here a_i and a_j are the areas of cells i and j adjacent to the edge m. Interestingly, since the pressure depends on the value of the cell area elasticity κ_A, the stability of isolated tension clusters must also depend on κ_A. To see the effect of cell area elasticity, we repeat the numerical calculations at various κ_A values. The dependence of G/σ on f_r is plotted for various κ_A values in Fig. 4(a). At $\kappa_A > 0$, G/σ suffers a slight dip at f_r^c but stays finite all the way until f_r below f_r^*. In general, as long as κ_A is finite, the rigidity transition does not shift. The case of $\kappa_A = 0$ is a singular limit where the rigidity transition shifts suddenly to f_r^c to coincide with the contact percolation transition. This confirms our hypothesis that when cells cannot exert pressure forces, the tension network can support mechanical rigidity only when rigid cells *physically come into contact*. In contrast, at $\kappa_A > 0$, stable tensions can be induced between rigid cells that are separated by a distance. We summarize these results in Fig. 4(b) and also incorporate the different scaling regimes for the solid phase when $\kappa_A > 0$. We are able to differentiate two types of solids: (i) when $\kappa_A > 0$, $f_r^* < f_r < f_r^c$, rigidity is strongly enhanced by heterogeneity [the lower branch in Fig. 1(b)], and (ii) when $\kappa_A > 0$, $f_r > f_r^c$, there is only weak enhancement of rigidity [the upper branch in Fig. 1(b)]. When $\kappa_A = 0$, heterogeneity has no effect.

Heterogeneity and cellular invasion.—We next focus on the effect of the heterotypic microenvironment on cell migration. A recent study [76] used a cellular Potts model to study tumor metastasis when cells are mismatched in their motility forces. As a complementary approach, here we use a dynamic vertex model [77,78] to simulate a tissue where only a single cell is invasive. The invading cell has a propulsive force v_0 along a polarity vector $\mathbf{n}$ which undergoes random rotational diffusion [55,79] at a slow rate. This mimics the directional motility of a metastatic cell under the influence of strong chemotactic signals [80]. In the tissue, each vertex ν evolves according to the overdamped equation of motion with a viscous drag Γ:

$$\Gamma\frac{d\mathbf{r}_\mu}{dt} = \begin{cases} -\frac{\partial \epsilon}{\partial \mathbf{r}_\mu} + v_0\mathbf{n}, & \text{vertices of invading cell,} \\ -\frac{\partial \epsilon}{\partial \mathbf{r}_\mu} & \text{for other vertices.} \end{cases} \quad (5)$$

Equation (5) is simulated with a fixed value $v_0 = 0.4$ and at various values of f_r. The mean total displacement of the invading cell is plotted as function of f_r in Fig. 5(a). The behavior at $f_r = 0$, 1 recapitulates results in the absence of heterogeneity [55], where a cell is either moving ($f_r = 0$) or stuck ($f_r = 1$). However, with heterogeneity tissues in the range of $0 < f_r < 1$ become accessible and cells moving through must interact with rigid as well as soft neighboring cells along its path of invasion. This results in a highly intermittent migration dynamics for the invading cell. To quantify the intermittency, we plot the kurtosis (defined in the SM [53]) in the displacement of the invading

cell [81] as a function of f_r. The displacement of the invading cells also shows a burstlike dynamics when the tissue is in the heterogeneous solid state [Fig. 5(b) and video in the SM [53]].

Discussion.—Our work suggests that tissue mechanics is determined not just by the average softness of the cells but on the statistical fluctuations in single-cell properties. The heterogeneity-driven rigidification can provide a possible resolution of the paradox regarding how soft cells can give rise to a tumor that is rigid at the tissue level [82]. As a simple example, we note that in the phase diagram [Fig. 3(c)], it is possible to transform from a fluid to a solid state by increasing μ (i.e., cells become softer overall) but at the same time increasing σ. Furthermore, our predictions show that the tissue mechanics is controlled by a single fraction f_r. This is consistent with a recent experimental finding [83] that a fraction of mesenchymal cells can serve as a control parameter in describing jamming properties, and that increasing mesenchymal fraction increases motility. There is also experimental evidence that heterogeneity can drive pulsating cancer cell migration in epithelial monolayers [24]. The intermittency we have observed in the dynamics of the invading cell in the heterogeneous solid state is highly reminiscent of such invasion behavior. With respect to imaging studies in epithelial sheets, we predict cell shape metrics (cellular aspect ratios [84] and cell shape indices [85]) (see the SM [53]) that can be used to distinguish between different mechanical phases. Tension profiles of a tissue can be directly obtained by laser-ablation experiments [44] or inferred from measurements of myosin concentration on cell edges [86], which can be compared to our theoretically predicted results. One possible avenue would be to perform the same percolation analysis on a tissue's cellular tension network.

We thank J. M. Schwarz, Bulbul Chakraborty, Madan Rao, Srikanth Sastry, Xingbo Yang, Jeffrey Fredberg, and Josef A. Käs for the insightful discussions. We acknowledge the support of the Northeastern University Discovery Cluster and the Indo-U.S. Virtual Networked Joint Center project titled "Emergence and Re-modeling of force chains in soft and Biological Matter No. IUSSTF/JC-026/2016.

*li.xinz@husky.neu.edu

[1] I. J. Fidler, Cancer Res. **38**, 2651 (1978).
[2] A. Marusyk and K. Polyak, Biochim. Biophys. Acta **1805**, 105 (2010).
[3] D. Hanahan and R. A. Weinberg, Cell **144**, 646 (2011).
[4] L. Gay, A. Baker, and T. Graham, F1000Research **5**, 238 (2016).
[5] A. Brock, H. Chang, and S. Huang, Nat. Rev. Genet. **10**, 336 (2009).
[6] Y. Shin, S. Han, E. Chung, and S. Chung, Integr. Biol. **6**, 654 (2014).
[7] M. Ackermann, Nat. Rev. Microbiol. **13**, 497 (2015).
[8] S. Bhatia, J. V. Frangioni, R. M. Hoffman, A. J. Iafrate, and K. Polyak, Nat. Biotechnol. **30**, 604 (2012).
[9] B. Claudi, P. Spröte, A. Chirkova, N. Personnic, J. Zankl, N. Schurmann, A. Schmidt, and D. Bumann, Cell **158**, 722 (2014).
[10] Q. Zhang and R. H. Austin, Annu. Rev. Condens. Matter Phys. **3**, 363 (2012).
[11] K. Anderson, C. Lutz, F. W. van Delft, C. M. Bateman, Y. Guo, S. M. Colman, H. Kempski, A. V. Moorman, I. Titley, J. Swansbury, L. Kearney, T. Enver, and M. Greaves, Nature (London) **469**, 356 (2011).
[12] M. Snuderl, L. Fazlollahi, L. P. Le, M. Nitta, B. H. Zhelyazkova, C. J. Davidson, S. Akhavanfard, D. P. Cahill, K. D. Aldape, R. A. Betensky, D. N. Louis, and A. J. Iafrate, Cancer Cell **20**, 810 (2011).
[13] F. Notta, C. G. Mullighan, J. C. Y. Wang, A. Poeppl, S. Doulatov, L. A. Phillips, J. Ma, M. D. Minden, J. R. Downing, and J. E. Dick, Nature (London) **469**, 362 (2011).
[14] A. Marusyk, V. Almendro, and K. Polyak, Nat. Rev. Cancer **12**, 323 (2012).
[15] M. Tian, Y. Li, W. Liu, L. Jin, X. Jiang, X. Wang, Z. Ding, Y. Peng, J. Zhou, J. Fan, Y. Cao, W. Wang, and Y. Shi, Nanoscale **7**, 12998 (2015).
[16] M. M. Yallapu, K. S. Katti, D. R. Katti, S. R. Mishra, S. Khan, M. Jaggi, and S C. Chauhan, Medicinal research reviews **35**, 198 (2015).
[17] A. Fritsch, M. Höckel, T. Kiessling, K. D. Nnetu, F. Wetzel, M. Zink, and J. A. Käs, Nat. Phys. **6**, 730 (2010).
[18] E. W. Morawetz, R. Stange, T. R. Kießling, J. Schnauß, and J. A. Käs, Convergent Sci. Phys. Oncol. **3**, 024004 (2017).
[19] M. Plodinec, M. Loparic, C. A. Monnier, E. C. Obermann, R. Zanetti-Dallenbach, P. Oertle, J. T. Hyotyla, U. Aebi, M. Bentires-Alj, R. Y. H. Lim, and C.-A. Schoenenberger, Nat. Nanotechnol. **7**, 757 (2012).
[20] Y. Fujii, Y. Ochi, M. Tuchiya, M. Kajita, Y. Fujita, Y. Ishimoto, and T. Okajima, Biophys. J. **116**, 1152 (2019).
[21] X. Guo, K. Bonin, K. Scarpinato, and M. Guthold, New J. Phys. **16**, 105002 (2014).
[22] G. Ciasca, T. E. Sassun, E. Minelli, M. Antonelli, M. Papi, A. Santoro, F. Giangaspero, R. Delfini, and M. De Spirito, Nanoscale **8**, 19629 (2016).
[23] H. T. Nia, H. Liu, G. Seano, M. Datta, D. Jones, N. Rahbari, J. Incio, V. P. Chauhan, K. Jung, J. D. Martin, V. Askoxylakis, T. P. Padera, D. Fukumura, Y. Boucher, F. J. Hornicek, A. J. Grodzinsky, J. W. Baish, L. L. Munn, and R. K. Jain, Nat. Biomed. Eng. **1**, 0004 (2016).
[24] M.-H. Lee, P.-H. Wu, J. R. Staunton, R. Ros, G. D. Longmore, and D. Wirtz, Biophys. J. **102**, 2731 (2012).
[25] C. Alibert, B. Goud, and J.-B. Manneville, Biol. Cell **109**, 167 (2017).
[26] D. T. Butcher, T. Alliston, and V. M. Weaver, Nat. Rev. Cancer **9**, 108 (2009).
[27] R. Sinkus, J. Lorenzen, D. Schrader, M. Lorenzen, M. Dargatz, and D. Holz, Phys. Med. Biol. **45**, 1649 (2000).
[28] T. Nagai and H. Honda, Philos. Mag. B **81**, 699 (2001).
[29] R. Farhadifar, J.-C. Röper, B. Aigouy, S. Eaton, and F. Jülicher, Curr. Biol. **17**, 2095 (2007).
[30] A. G. Fletcher, M. Osterfield, R. E. Baker, and S. Y. Shvartsman, Biophys. J. **106**, 2291 (2014).

[31] D. B. Staple, R. Farhadifar, J. C. Röper, B. Aigouy, S. Eaton, and F. Jülicher, Eur. Phys. J. E **33**, 117 (2010).
[32] D. Bi, J. H. Lopez, J. M. Schwarz, and M. L. Manning, Nat. Phys. **11**, 1074 (2015).
[33] S. Kim and S. Hilgenfeldt, Soft Matter **11**, 7270 (2015).
[34] D. L. Barton, S. Henkes, C. J. Weijer, and R. Sknepnek, PLoS Comput. Biol. **13**, e1005569 (2017).
[35] M. Moshe, M. J. Bowick, and M. C. Marchetti, Phys. Rev. Lett. **120**, 268105 (2018).
[36] S. Henkes, K. Kostanjevec, J. M. Collinson, R. Sknepnek, and E. Bertin, arXiv:1901.04763.
[37] D. M. Sussman, J. M. Schwarz, M. C. Marchetti, and M. L. Manning, Phys. Rev. Lett. **120**, 058001 (2018).
[38] E. Teomy, D. A. Kessler, and H. Levine, Phys. Rev. E **98**, 042418 (2018).
[39] A. Boromand, A. Signoriello, F. Ye, C. S. O'Hern, and M. D. Shattuck, Phys. Rev. Lett. **121**, 248003 (2018).
[40] B. Li and S. X. Sun, Biophys. J. **107**, 1532 (2014).
[41] L. Hufnagel, A. A. Teleman, H. Rouault, S. M. Cohen, and B. I. Shraiman, Proc. Natl. Acad. Sci. U.S.A. **104**, 3835 (2007).
[42] S. M. Zehnder, M. Suaris, M. M. Bellaire, and T. E. Angelini, Biophys. J. **108**, 247 (2015).
[43] G. W. Brodland, Appl. Mech. Rev. **57**, 47 (2004).
[44] M. S. Hutson, Y. Tokutake, M.-S. Chang, J. W. Bloor, S. Venakides, D. P. Kiehart, and G. S. Edwards, Science **300**, 145 (2003).
[45] M. Rauzi, P. Verant, T. Lecuit, and P.-F. Lenne, Nat. Cell Biol. **10**, 1401 (2008).
[46] G. W. Brodland, V. Conte, P. G. Cranston, J. Veldhuis, S. Narasimhan, M. S. Hutson, A. Jacinto, F. Ulrich, B. Baum, and M. Miodownik, Proc. Natl. Acad. Sci. U.S.A. **107**, 22111 (2010).
[47] K. K. Chiou, L. Hufnagel, and B. I. Shraiman, PLoS Comput. Biol. **8**, e1002512 (2012).
[48] S. Ishihara and K. Sugimura, J. Theor. Biol. **313**, 201 (2012).
[49] S. Ishihara, K. Sugimura, S. J. Cox, I. Bonnet, Y. Bellaïche, and F. Graner, Eur. Phys. J. E **36**, 45 (2013).
[50] G. W. Brodland, J. H. Veldhuis, S. Kim, M. Perrone, D. Mashburn, and M. S. Hutson, PLoS One **9**, e99116 (2014).
[51] L. Yan and D. Bi, Phys. Rev. X **9**, 011029 (2019).
[52] X. Yang, D. Bi, M. Czajkowski, M. Merkel, M. L. Manning, and M. C. Marchetti, Proc. Natl. Acad. Sci. U.S.A. **114**, 12663 (2017).
[53] See Supplemental Material at http://link.aps.org/supplemental/10.1103/PhysRevLett.123.058101, which includes Ref. [54], for additional calculations, methods, and a simulation movie on cellular invasion.
[54] C. E. Maloney and A. Lemaître, Phys. Rev. E **74**, 016118 (2006).
[55] D. Bi, X. Yang, M. C. Marchetti, and M. L. Manning, Phys. Rev. X **6**, 021011 (2016).
[56] D. Sánchez-Gutiérrez, M. Tozluoglu, J. D. Barry, A. Pascual, Y. Mao, and L. M. Escudero, EMBO J. **35**, 77 (2016).
[57] K. A. Brakke, Exp. Math. **1**, 141 (1992).
[58] E. Bitzek, P. Koskinen, F. Gähler, M. Moseler, and P. Gumbsch, Phys. Rev. Lett. **97**, 170201 (2006).
[59] R. Byrd, P. Lu, J. Nocedal, and C. Zhu, SIAM J. Sci. Comput. **16**, 1190 (1995).
[60] U. Gropengiesser and D. Stauffer, Physica (Amsterdam) **210A**, 320 (1994).
[61] C.-K. Hu, J. Phys. A **27**, L813 (1994).
[62] D. P. Landau, Phys. Rev. B **13**, 2997 (1976).
[63] D. P. Landau, Phys. Rev. B **14**, 255 (1976).
[64] C.-K. Hu, C.-Y. Lin, and J.-A. Chen, Physica (Amsterdam) **221A**, 80 (1995).
[65] J.-P. Hovi and A. Aharony, Phys. Rev. E **53**, 235 (1996).
[66] D. Weaire and S. Hutzler, *The Physics of Foams* (Clarendon Press, Oxford, 2001).
[67] D. Bi, J. H. Lopez, J. M. Schwarz, and M. L. Manning, Soft Matter **10**, 1885 (2014).
[68] S. Feng and P. N. Sen, Phys. Rev. Lett. **52**, 216 (1984).
[69] D. J. Jacobs and M. F. Thorpe, Phys. Rev. Lett. **75**, 4051 (1995).
[70] D. J. Jacobs and M. F. Thorpe, Phys. Rev. E **53**, 3682 (1996).
[71] W. Tang and M. F. Thorpe, Phys. Rev. B **37**, 5539 (1988).
[72] S. Ostojic, E. Somfai, and B. Nienhuis, Nature (London) **439**, 828 (2006).
[73] V. K. Shante and S. Kirkpatrick, Adv. Phys. **20**, 325 (1971).
[74] H.-P. Hsu and M.-C. Huang, Phys. Rev. E **60**, 6361 (1999).
[75] A. M. Becker and R. M. Ziff, Phys. Rev. E **80**, 041101 (2009).
[76] A. Hallou, J. Jennings, and A. J. Kabla, R. Soc. Open Sci. **4**, 161007 (2017).
[77] M. F. Staddon, D. Bi, A. P. Tabatabai, V. Ajeti, M. P. Murrell, and S. Banerjee, PLoS Comput. Biol. **14**, e1006502 (2018).
[78] J. A. Mitchel, A. Das, M. J. O'Sullivan, I. T. Stancil, S. J. DeCamp, S. Koehler, J. P. Butler, J. J. Fredberg, M. A. Nieto, D. Bi, and J.-A. Park, https://doi.org/10.1101/665018.
[79] Y. Fily and M. C. Marchetti, Phys. Rev. Lett. **108**, 235702 (2012).
[80] A. G. Clark and D. M. Vignjevic, Curr. Opin. Cell Biol. **36**, 13 (2015).
[81] A. Das, A. Polley, and M. Rao, Phys. Rev. Lett. **116**, 068306 (2016).
[82] L. Oswald, S. Grosser, D. M. Smith, and J. A. Käs, J. Phys. D **50**, 483001 (2017).
[83] M. Gamboa Castro, S. E. Leggett, and I. Y. Wong, Soft Matter **12**, 8327 (2016).
[84] L. Atia, D. Bi, Y. Sharma, J. A. Mitchel, B. Gweon, S. A. Koehler, S. J. DeCamp, B. Lan, J. H. Kim, R. Hirsch, A. F. Pegoraro, K. H. Lee, J. R. Starr, D. A. Weitz, A. C. Martin, J.-A. Park, J. P. Butler, and J. J. Fredberg, Nat. Phys. **14**, 613 (2018).
[85] J.-A. Park *et al.*, Nat. Mater. **14**, 1040 (2015).
[86] S. J. Streichan, M. F. Lefebvre, N. Noll, E. F. Wieschaus, and B. I. Shraiman, eLife **7**, e27454 (2018).